CALICE Analysis Note CAN-039
November, 2012

Analysis of Tungsten-DHCAL Data from the CERN Test Beam

The CALICE Collaboration[1]

Abstract

This note reports on the status of the analysis and preliminary results of the large CALICE Digital Hadron Calorimeter prototype (W-DHCAL) from tests in the CERN test beams. In these tests, the W-DHCAL consisted of 39 layers instrumented with Resistive Plate Chambers (RPCs), interleaved with 1 cm thick tungsten absorber plates. In addition, a steel plate absorber structure located behind the main stack and also instrumented with layers of RPCs, served as a tail catcher. The prototype was tested in the PS beam (1 – 10 GeV/c) and, subsequently, in the SPS H8 beam line (10 – 300 GeV). The note describes the setup, the test beams, and the trigger. It discusses the event selection and the measured response to muons, pions, protons and electrons. To help understand certain features of the data, a selection of the results is compared to predictions from detailed Monte Carlo simulations of the set-up and the RPC response.

1 Corresponding author: José Repond, repond@hep.anl.gov

1. Introduction

This note describes the preliminary analysis of events collected with the CALICE Digital Hadron Calorimeter prototype (W-DHCAL) in the CERN test beams. These tests followed several periods of extensive testing in the Fermilab test beam [1-3], using steel absorber plates. The tests at CERN have been performed with tungsten absorber plates in the main stack. The use of tungsten absorber plates reduces the shower leakage at higher energies, without increasing the actual depth of the calorimeter. Similar tests have been reported with the CALICE AHCAL, where measurements with steel [4] and tungsten absorber plates [5] had been performed. In both cases the main stack was supplemented with a tail catcher, in the following named TCMT (Tail Catcher and Muon Tracker), containing steel absorber plates. The W-DHCAL was tested in both the PS and the SPS beams.

2. Brief description of the W-DHCAL as configured for the CERN test beams

The W-DHCAL consisted of 54 active layers, equipped with Resistive Plate Chambers (RPCs) and interleaved with absorber plates. The first 39 of these layers were inserted into the CERN tungsten absorber structure [5], featuring 1 cm thick tungsten plates and in the following named the 'main stack'. The distance between the plates was 15 mm, of which 12.85 mm were occupied by the cassette structure of the active layers. Each cassette featured a 2 mm copper plate and a 2 mm steel plate, which is to be added to the effective absorber thickness of each layer. Thus each layer corresponded to approximately 3.3 radiation lengths X_0 or 0.14 nuclear interaction lengths λ_I.

A photograph of the main stack before cabling is shown in Fig. 1. It contained 117 individual RPCs and 359,424 readout channels. During the data taking, the main stack was placed inside a double-walled tent, cooled by two 4 kW and one 7 kW air conditioning units. The temperature inside the stack was thus stabilized and averaged around 30^0 C.

Figure 1. Photograph of the main W-DHCAL stack before cabling. The entire installation was placed on a platform, which facilitated the move from one test beam to the other.

The remaining 15 layers were inserted into a steel structure, the TCMT, which was located 23.5 cm behind the main stack. The first 8 absorber plates each measured 2 cm and the remaining plates each 10

cm. The active elements of the TCMT were identical to the ones of the main stack. The first active layer was placed after the first 2 cm absorber plate. The TCMT was cooled with fans positioned underneath and on top of the structure. Due to the larger gaps between absorber plates and the resulting improved air flow compared to the main stack, cooling with fans appeared to be sufficient, but resulted in some temperature fluctuations during the course of a running campaign. In the first (second) part of the TCMT each layer corresponded to approximately 1.6 X_0 or 0.16 λ_I (6.1 X_0 or 0.63 λ_I).

With 39 + 15 = 54 layers, each with 96 × 96 pads, the W-DHCAL counted a world record 497,664 readout channels for both calorimetry and RPC systems. After the move to the SPS H8 beam line, the last active layer of the TCMT was scavenged to replace faulty RPCs in the main stack. This reduced the total number of active layers to 53 and the number of readout channels to 488,448. The total thickness of the 54-layer W-DHCAL (main stack and TCMT) corresponded to approximately 183 radiation lengths or 11.1 nuclear interaction lengths.

The RPCs were flushed with a three component gas mixture, Tetrafluorethane : Isobutane : Sulfur hexafluoride, with the volumetric ratios of 94.5 : 5.0 : 0.5. The pressure inside the chambers was maintained at atmospheric pressure. The chambers were operated at a default high voltage of 6.0 kV. During the extended data taking periods the high voltage on a small number of chambers was increased, in order to maintain a high MIP detection efficiency in all chambers. The default voltage for the second period at the SPS was raised to 6.1 kV.

The RPCs were read out with 1 × 1 cm^2 pads, to which a single threshold was applied (thus the term ‘Digital’ in W-DHCAL). The electronic readout was integrated into the active layers and was based on the DCAL III chip, developed [6] specifically for the W-DHCAL. Each DCAL chip was connected to 8 × 8 pads and transferred its data to a data concentrator located on the edge of the readout board, but off the active area of the RPCs. Individual layers were read out by six Readout boards, each containing 4 × 6 = 24 DCAL chips.

The W-DHCAL data consisted of a timestamp with a 100 ns resolution and the hit pattern of the 8 × 8 pads. For each trigger the data acquisition recorded the time-stamp of the trigger and hit patterns together with their time-stamps in seven consecutive time bins. The first two of these corresponded to times before the particle triggering the data acquisition reached the detector, thus providing a baseline measurement of the noise level.

In the following, the response is defined as a linear sum (without weights) of the hits in the W-DHCAL and the two sections of TCMT.

3. The PS and SPS beam lines

The PS beam line offers beam in the momentum range of 1 – 10 GeV/c. The particles arrived in 400 millisecond spills. During the two week run period the number of spills per 45 second intervals varied from one to three. Due to the limited rate capability of RPCs [7], the beam intensity was kept at or below about 500 triggers/spill. Electrons were tagged with a pair of Cerenkov counters, filled with CO_2. The pressures were adjusted to either select electrons versus muons/pions (for negative beams) or to select positrons versus muons/pions versus protons for positive beams. Three drift chambers provided precise tracking of the beam particles, but are not used in the present analysis. Figure 2 shows

a sketch of the beam line.

The SPS beam line offers beam in the momentum range of 10 – 300 GeV/c. The particles arrive in 9.7 second spills every 45 – 60 seconds. A pair of Cerenkov counters, filled with helium, was used to distinguish electrons from muons/pions up to 25 GeV/c and pions from protons up to 200 GeV/c. Depending on the beam momentum selection, the beam intensity was limited to 250 – 500 triggers/spill. The fraction of pions in the beam could be enhanced by inserting an 18 mm lead foil far upstream, after the momentum selection.

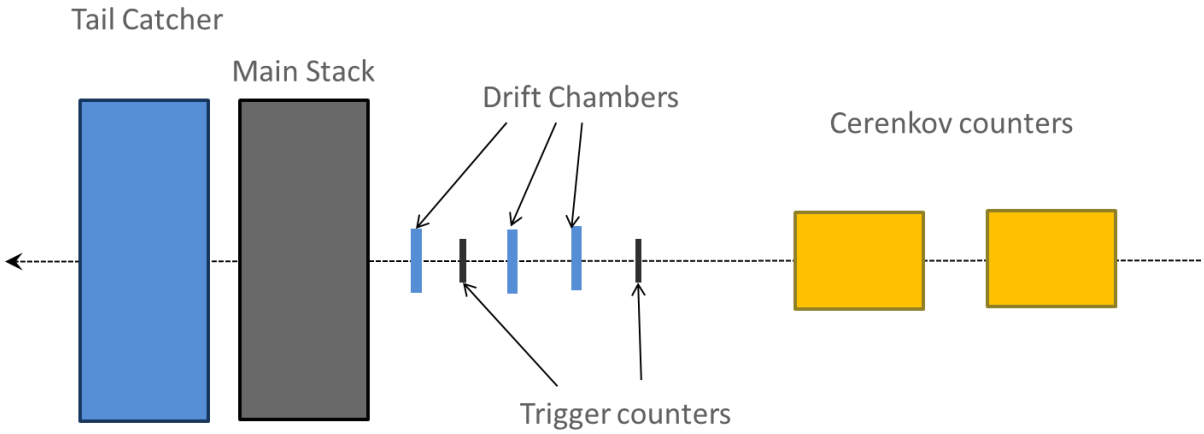

Figure 2. Sketch of the setup in the beam line. Dimensions not to scale.

Figure 3 shows a photograph of the W-DHCAL (main stack and TCMT) in the PS beam line, after cabling. The distance between the last layer in the main stack and the first layer in the TCMT was approximately 23.5 cm.

Figure 3. Photograph of the W-DHCAL (including main stack and TCMT) in the PS beam line, after cabling.

4. Trigger and data taking

The data acquisition was triggered by two scintillation counters, with an area of 10 × 10 cm^2, located

upstream of the W-DHCAL, see Fig.2. The counters were placed at a position corresponding to the center of the main stack.

The beam operated for 24 hours a day. The PS data taking period started on May 16th, 2012 and lasted for two weeks. The SPS data taking started on June 4th, 2012 and was divided into one period of two weeks plus two periods of one week each – the final of which will be in November 2012. Table I summarizes the number of events collected at the PS and in the first two periods at the SPS. Over the three different data taking periods a grand total of about 30 Million events were written to disk. Since no charge injection or other calibration events were collected during this time, this number (and the numbers in Table I) correspond to actual events triggered by the pair of scintillation counters.

Table I. Number of events collected with the various momentum selections and with or without additional material in the beam line.

Polarity	**Momentum [GeV/c]**	**18 mm Pb absorber**	**No Pb absorber**	**Beam blocker**	**Total**
Negative	1		540,660		540,660
	2		964,361		964,361
	3		1,006,185		1,006,185
	4		1,030,302		1,030,302
	5		1,185,235		1,185,235
	6		1,268,235		1,268,235
	7		1,546,744		1,546,744
	8		1,196,804		1,196,804
	9		2,044,224		2,044,224
	10		1,007,922		1,007,922
	12		300,666		300,666
	15	305,735			305,735
	20	465,904	438,356		904,260
	30	594,132	410,731		1,004,863
	40	510,736	303,020		813,756
	50	886,201			886,201
	60	497,739			497,739
	80	722,268			722,268
	100	526,323	64,658		590,981
	120	505,465			505,465
	180	123,448			123,448
	210	350,302			350,302
	240	283,554			283,554
	270	206,733			206,733
	300	436,133		704,141	1,140,274
	Total	**6,414,673**	**13,308,103**	**704,141**	**20,426,917**
Positive	4		1,137,898		1,137,898
	6		655,638		655,638
	8		527,234		527,234
	10		359,768		359,768
	60		10,125		10,125
	150	289,888	230,515		520,403
	180	303,917	211,482	4,920,679	5,436,078
	Total	**593,805**	**3,132,660**	**4,920,679**	**8,647,144**
Grand total		**7,008,478**	**16,440,763**	**5,624,820**	**29,074,061**

To expose the W-DHCAL to a pure muon beam a 3 m thick iron beam blocker was inserted into the beam circa 30 m upstream the experimental setup. The resulting muon beam had a diameter of ~ 50 cm at the location of the experiment. The data with the beam blocker were collected with triggers from a pair of 30 × 30 cm^2 scintillation counters, one placed upstream of the main stack and the other downstream of the TCMT. These events contain almost exclusively through-going muons.

To illustrate the quality of the data taken, Figure 4 shows two sample events collected in the SPS beam with a negative polarity and a 300 GeV/c momentum selection.

Additional information on the beam setup, detector platform and trigger telescope can be found in [8].

5. Monte Carlo simulation

In this note several experimental results are compared to Monte Carlo simulations. The simulations are based on GEANT4 [9] and include a detailed simulation of the absorber stack and its active elements. Hadronic showers are modeled using QGSP_Bertini. The response of the RPCs was tuned to reproduce the measured response to muons [1]. The muon data used for the tuning was recorded at Fermilab in 2010 and no attempt was made to retune the response to the different operational conditions, such as temperature and ambient pressure, at CERN. In this note the purpose of comparing the experimental data to simulations is to gain understanding of the features of the data. The aim was not yet to provide detailed comparisons with predictions.

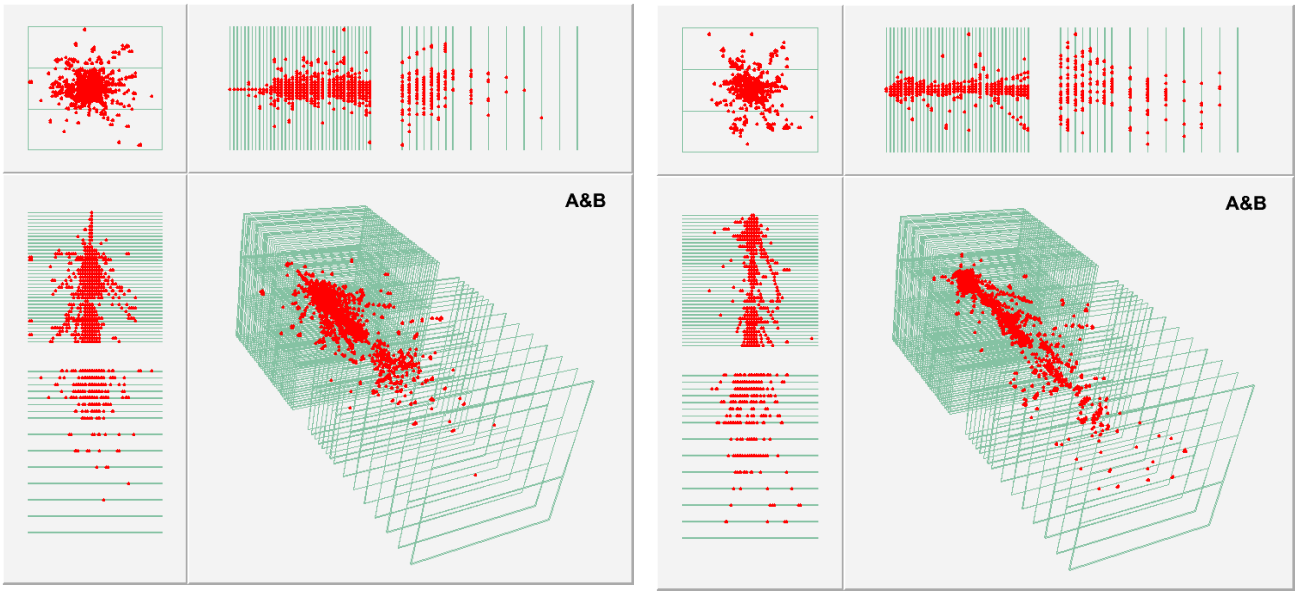

Figure 4. Different views of two events collected at 300 GeV/c negative beam.

6. Reconstruction and event cleaning

The events were reconstructed offline from the binary files written by the data acquisition system. For

every trigger, the data acquisition recorded seven consecutive time-stamps and their corresponding hit patterns. Hit patterns containing no hits were zero-suppressed at the data concentrator stage. As the hit patterns stored in the binary files were not all time-sorted, the main task of the event builder was to sort the hit patterns by time-stamp and to group the hit patterns from various parts of the detector into events. The output of the event builder was an ASCII-file with four entries per line: timestamp, x, y, and z of each hit. Both the timestamp (in units of 100 ns) and the coordinates were given in integers. The z coordinate corresponded to the layer number, rather than the distance in cm.

During a run the data acquisition also counted the number of spills. This information and the Cerenkov counter bits were stored in each event header.

For reasons not entirely understood at this point, the pads close to the ground connection of the RPCs showed a high rate of noise hits. This rate fluctuated from RPC to RPC, showing excessive rates for a number of chambers. In order to reduce the overall number of random hits in the triggered events, hits in an area of $\Delta x \times \Delta y = 5 \times 2$ cm^2 around the grounding strip of each RPC were removed offline from the record. The grounding strips were located on one of the shorter edges of the chambers. Thus, removing any hits in these areas had a minimal effect on the measurement of showers in the W-DHCAL.

Figure 5 shows the difference between the trigger time-stamp and the time-stamps of individual hits in reconstructed events for a given run. As expected the plot shows seven bins with non-zero entries. The first two entries correspond to times before the particle/shower enters the W-DHCAL and can be used to measure the random noise rate. Most hits appear in the following two bins[2], with some hits (approximately 12.6%) being recorded in the remaining three bins. To reduce the effects of hits related to random discharges in the RPCs, the hits in the last three time bins have been discarded from any further analysis.

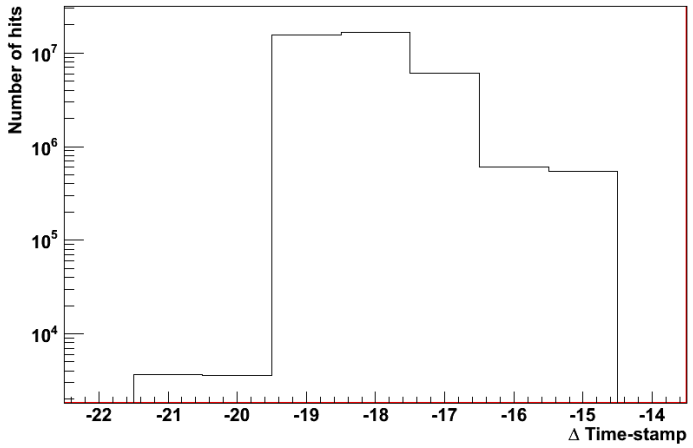

Figure 5. Distribution of the difference between the trigger time-stamp and the hit time-stamps. Each bin corresponds to 100 ns.

[2] During the data acquisition the DCAL chip stores the hit patterns in a digital pipeline with 20 slots. The data are moved from slot to slot with each clock cycle. A positive trigger decision will capture the data at the end of the pipeline and transfer them to a write-out buffer. The distribution in Fig. 5 peaks at -18, which means that the trigger decision took of the order of (20-18)×100 ns = 200 ns to reach the front-end.

Occasionally, hits with the same coordinate, but different time-stamps, appeared in the event record. To avoid double counting, one of these hits was removed from the record.

7. Identification and rejection of box events

With the higher energies available at the SPS, a significant fraction of the events showed parts of a front-end board or its borders light up. The reasons for this effect are not entirely understood, but are most likely related to shifts in the ground baseline in events with large numbers of avalanches in the RPCs. Examples of individual layers with such 'boxes' are shown in Fig. 6. An algorithm was developed to eliminate events with such boxes. The performance of the algorithm was tuned by scanning large numbers of events with layers where boxes had or had not been identified. The efficiency and mis-identification rate was estimated by scanning events and amount to approximately 97% and 3%, respectively. Both the failed-to-be-identified and mis-identified events have in general boxes with only few hits, thus introducing a negligible bias on the event selection. When applied to simulated 100 GeV pions in the W-DHCAL, only 24 out of 10,000 events are wrongly identified as containing a box.

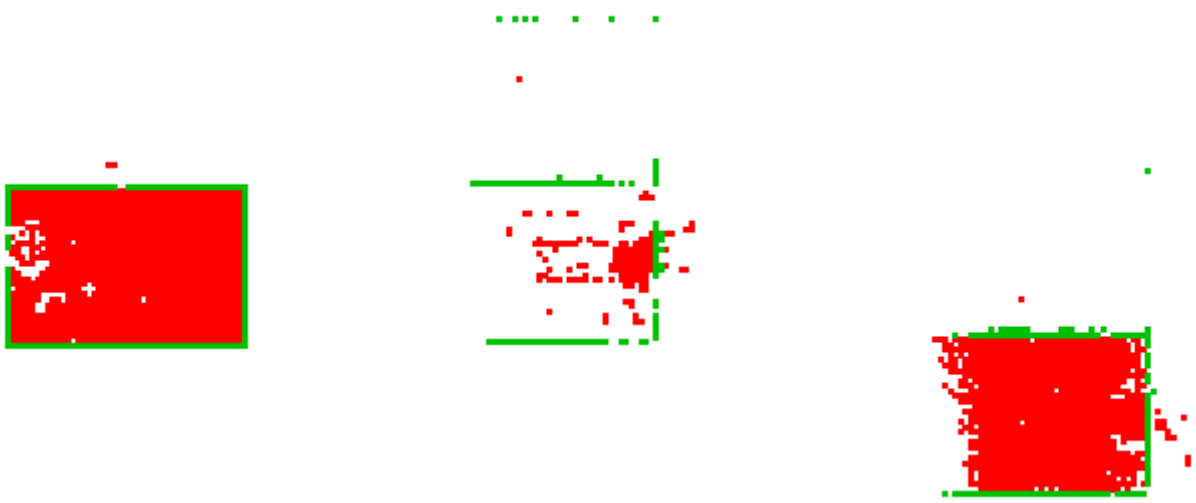

Figure 6. Hits in three different layers (from different events) showing un-physical hits related to the geometry of the front-end boards, so-called boxes. The hits on the inside (on the border) of the boards are shown in red (green).

Based on the above algorithm, Fig. 7 shows the observed fraction of events with identified boxes in runs taken with the 18 mm lead absorber inserted (pion runs). Below 100 GeV the fraction is well below 1%, but then rises above 30% at 300 GeV. The large scattering of the points compared to the statistical precision of the data is most likely caused by the varying beam intensity of these particular runs. Events with identified boxes are rejected from further analysis.

8. Determination of the Interaction Layer, Barycenter and Hit Density

Algorithms to identify the interaction layer (the layer at which a hadron starts showering) IL, the

barycenter BC and the hit density R of an event were developed. These quantities were used to select events and identify the incident particles

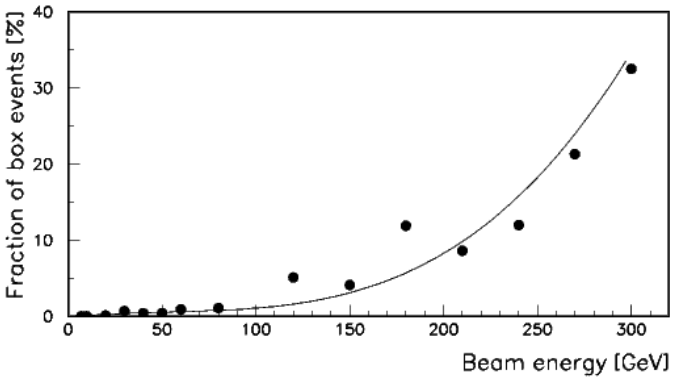

Figure 7. Fraction of box events as function of beam energy for pion runs. The line is an empirical fit to a fourth order polynomial and only serves to guide the eye.

Several different criteria were explored to identify the interaction layer IL. In simulation, the best results were obtained by an algorithm identifying as the interaction layer the first layer of two consecutive layers with more than three hits. Figure 8 shows the correlation between the generated (as identified by the GEANT4 program) and the reconstructed IL (left) and the difference between the two (right) for 100 GeV pion showers. Using the same algorithm, similar results were also obtained at lower energies.

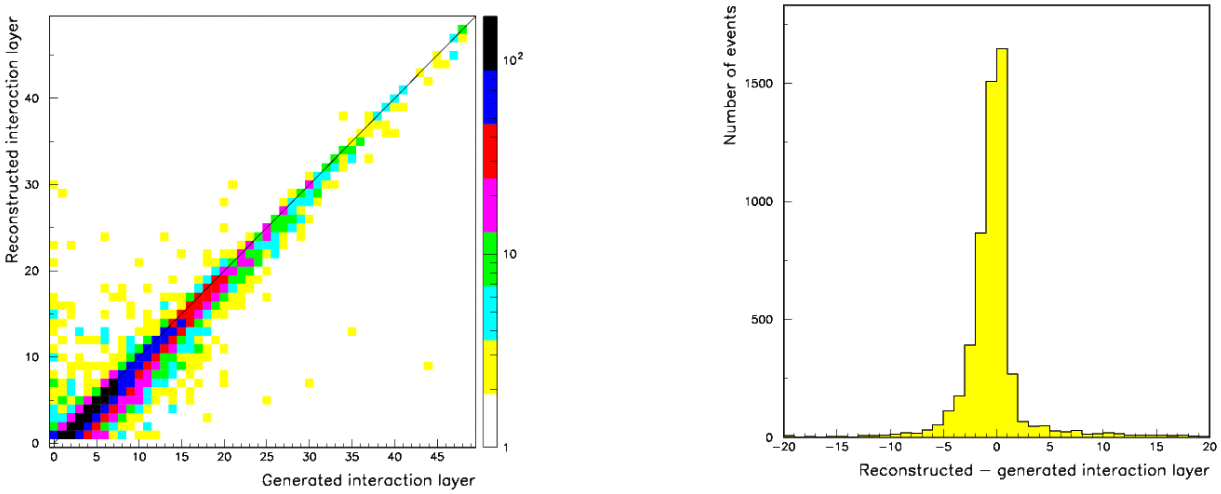

Figure 8. Left: Reconstructed versus generated interaction layer for 100 GeV/c pion showers. The color scale shows the event rate. Right: Difference of reconstructed and generated interaction layers.

The barycenter *BC* of an event was calculated as the sum over all layer indices, weighted by their number of hits, and divided by the total sum of hits

$$BC = \frac{\sum_{i=0}^{53} i \cdot N_i}{\sum_{i=0}^{53} N_i}$$

where N_i represents the number of hits in layer i.

The hit density, *R*, was defined as the average number of hits per active layer, i.e. a layer with at least one hit[3]

$$R = \frac{\sum_{i=0}^{53} N_i}{\sum_{i=0}^{53} \mathrm{sgn}(N_i)},$$

where sgn(N_i) is defined as +1 for N_i>0, 0 for N_i=0. Figure 9 shows the distribution of the hit density variable for a 80 GeV negative beam data sample with the 18 mm lead absorber inserted. Values of *R* below 5 correspond to through-going muons, whereas larger values correspond to pions. (Due to the lead absorber, this data sample contained only a negligible contamination from electrons. Electrons would result in large values of *R*.) For lower beam momenta the distribution of *R* values moves to the left.

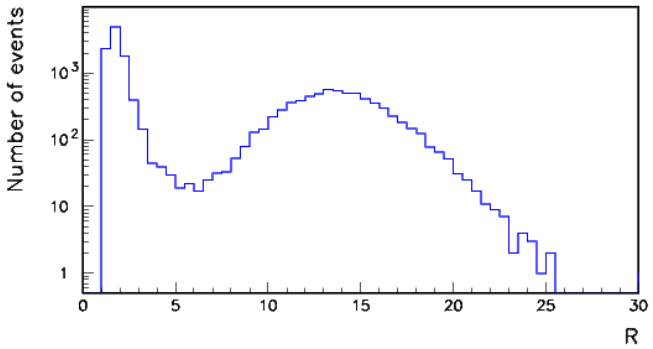

Figure 9. Hit density *R* for a negative 80 GeV run with the 18 mm lead absorber inserted into the beam line.

9. Event selection

The event selection is straightforward and simple. To obtain a sample of clean events without obvious beam or readout related problems, events with

- an identified box (in any layer)
- at least 6,000 hits overall (at the highest energies of the SPS, the average hit count is approximately 1,700) or
- no hits in the record

[3] The noise rate was similar to the one measured at the Fermilab testbeam, corresponding to a fraction of a hit per triggered event.

were discarded.

Hits in each layer were clustered using a simple nearest-neighbor clustering algorithm. In this algorithm, hits with a common side are clustered together to form a cluster. To reduce the number of events with interactions upstream of the W-DHCAL, all events were required to have exactly one cluster in the first layer (layer 0) with at most 11 hits.

In addition, cuts were applied to select separate samples of through-going muons, electrons, pions or protons. The cuts are summarized in Table II. A few comments are in order here:

- The Cerenkov counters, denoted as C_1 and C_2, were very efficient in tagging electrons or pions.
- For negative (positive) beams the Cerenkov counters were in general set to distinguish between electrons and pions/muons (pions/muons/protons). For positive beams the second Cerenkov was operated at a pressure to distinguish positive pions and protons. The pressures varied with the momentum selection.
- As mentioned above, the hit density values tend to be smaller at lower momenta. As a result the pion selection used a sliding cut from R>2.0 to R>5.0, depending on the momentum selection of the beam.
- For energies above 15 GeV a lead absorber in the beam line was used to remove electrons. For energies up to 25 GeV Cerenkov counters were used to distinguish electrons from muons/pions.
- The additional cut on N_0 (the number of hits in layer 0) to select electrons was introduced to reduce the contamination from pions in the sample.
- The cut on the IL>2 for pions at energies above 3 GeV was introduced to eliminate any remaining contamination from electrons/positrons.

Table II. Additional cuts to select specific particle types. C_1 and C_2 correspond to the upstream and downstream Cerenkov counters. BC, R, and IL are defined as the barycenter, the R value and the reconstructed interaction layer of the event.

Particle	Cerenkov	*BC*	*R*	*IL*	N_0	$\sum_{i=last-4}^{last} N_i$	$\sum_{i=0}^{last} N_i$
μ		>20	<3.0	-		>0	>10
$e^{\pm}$	$C_1 \cdot C_2=1$	<8	>4.0 for E>12 GeV	-	>4 for E>12 GeV	-	-
π^-	$C_1+C_2=0$	-	>2.0 – 5.0	>2 for E>3 GeV		-	-
π^+	$C_1=0$ and $C_2=1$ ($p \leq 10$ GeV/c) $C_1 \cdot C_2=1$ (p > 10 GeV/c)	-	>2.0 – 5.0	>2 for E>3 GeV		-	-
p	$C_1+C_2=0$	-	>2.0 – 5.0			-	

10. Effects of high particle rates

As a result of the current flowing through the chambers, at high beam intensities the effective high

voltage in the gas gap of the RPCs decreases as a function of event time within a spill [7]. This effect leads to a decrease in overall response. For a constant beam intensity during a spill, the decrease in efficiency can be described by an exponential with the time constant of the order of one second [7]. Since the spill length at the PS is 0.3 s this decrease was not observed. However, at the SPS the spill length is 9.7 s and the effect is clearly visible. Figure 10 shows a profile plot of the average peak position of the response to 300 GeV negative pions. The data are fit to the sum of an exponential and a constant. Over the length of the spill the peak position decreases by 5.9%. In principle, this effect can be corrected for offline. However, such corrections have not yet been applied.

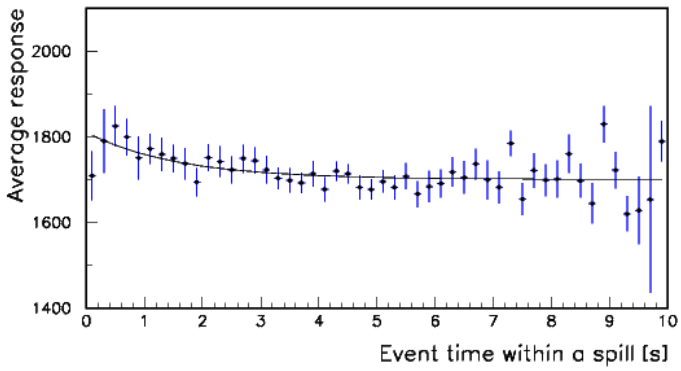

Figure 10. Average response to 300 GeV negative pions as function of event time within a spill. The line is the result of a fit to the sum of an exponential and a constant, as proposed in [7].

11. Measurements at the CERN PS

The PS delivers beams in the momentum range from 1 to 10 GeV/c. Data were collected both with positive and negative beams. Electrons were tagged efficiently using the upstream Cerenkov counters. The data selection applied a minimal set of cuts (see section 9), in order to avoid a bias of the response.

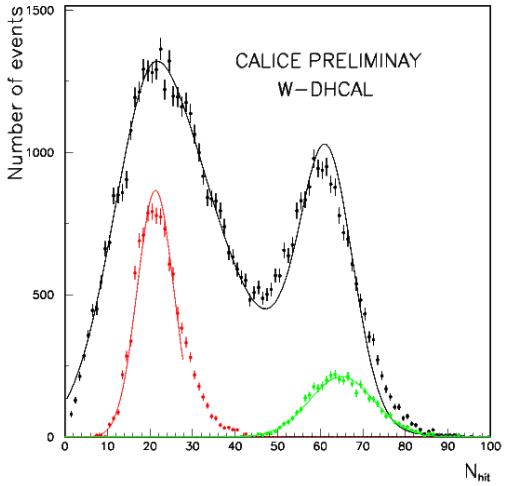

Figure 11. Response for a 2 GeV/c negative beam as function of the number of hits.. Black dots are data with pion selection, red dots for electron selection and green dots for through-going muons. The solid lines are Gaussian fits (see text).

As an example, Fig. 11 shows the response obtained with a negative 2 GeV/c beam. Through-going muons result in a response around 65 hits, corresponding to an average 1.2 hits/layer, and which is adequately fit by a Gaussian function. The response of electrons peaks at a lower value, around 21 hits, and shows an asymmetric tail towards larger values. The pion selection results in a response with two peak, the peak around 60 hits being due to muons ranging out in the W_DHCAL. To understand the observed two-peak structure in detail, the response of negative muons and pions with a momentum of 2 GeV/c was simulated. As shown in Fig. 12 the response to pions (muons) results in asymmetric peaks around 25 (60) hits. These response curves were fit with a modified Gaussian with variable width σ [10], where e.g. a tail towards larger values is emulated by

$$x < \mu \qquad \sigma = \sigma_0$$
$$x \geq \mu \qquad \sigma = \sigma_0 + a(x-\mu)^b$$

with σ_0, μ (the peak position), a and b as free parameters. A similar function can be used to fit a tail towards lower values.

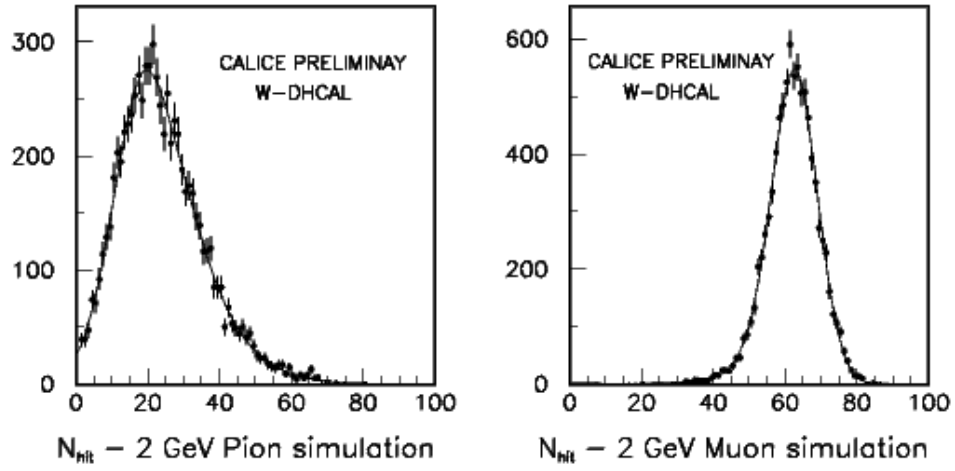

Figure 12. Simulated response of 2 GeV/c negative pions (left) and muons (right). The curves are modified Gaussian functions with variable widths (see text), fitted to the data.

In a two-component fit, the measured response to 2 GeV/c pions and muons of Fig.11 were fit to their simulated responses. To obtain a satisfactory fit and since the data have not yet been calibrated, the simulated response to pions was multiplied by a factor of 1.1.

The double peak structure visible at 2 GeV/c was also observed in the 1 GeV/c data, but not at beam momenta momenta above 3 GeV/c, since higher momentum muons do not range out in the W-DHCAL.

The responses to the various particles in the beam were each fitted with (symmetric) Gaussian functions. Figure 13 shows the mean response as function of beam momentum for the various particles in the beam. As the response of individual RPCs as function of time has not yet been calibrated, the response of through-going muons shows some fluctuations. The responses to positive pions, negative pions and protons (after correction for the rest mass) show reasonable agreement. The response to

electrons and positrons is significantly smaller than the response to hadrons. In other words, the W-DHCAL with 1 x 1 cm^2 readout pads is strongly overcompensating, even at these low energies. This is in contrast to what was observed with steel absorber plates, where the response is compensating in the range of 8 – 10 GeV/c and undercompensating (overcompensating) below (above) [3].

The response to electrons, pions and protons shows some deviations from a linear response. These are much more pronounced than what was observed with steel absorber [3] and is a direct consequence of the higher density of particles in a stack with tungsten absorber. In general, to extend the linearity to higher momenta, smaller pad sizes, say of the order of 0.5 × 0.5 cm^2, are required [11]. The response to electrons, pions and protons was fit empirically with a power law, $a \cdot p^b$, where p is the beam momentum and a and b are free parameters. Table III lists the values of the fitted parameters. A linear response would correspond to b = 1.

Figure 14 shows the resolution defined as relative width of the Gaussians versus beam momentum. The widths for both electrons and pions have been corrected for the observed non-linearity of the response (typically a 10% correction). As expected the through-going muon response shows a constant width, independent of the momentum selection. At momenta below 6 GeV/c the pion distributions showed small, asymmetric tails (decreasing with higher momenta), which were excluded from the fit ranges. The hadron and electron responses show the characteristic behavior of calorimeters. Fits of the quadratic sum of a stochastic (proportional to $1/\sqrt{E}$) and constant term seem to describe the measurements adequately. Table IV lists the results of the fits. Errors on the fitted parameters are not given, since systematic errors have not yet been evaluated. The large constant terms, in particular for electrons, are related to the saturation effects mentioned above. Both Fig. 14 and Table IV also show the result of a fit to the stochastic term only.

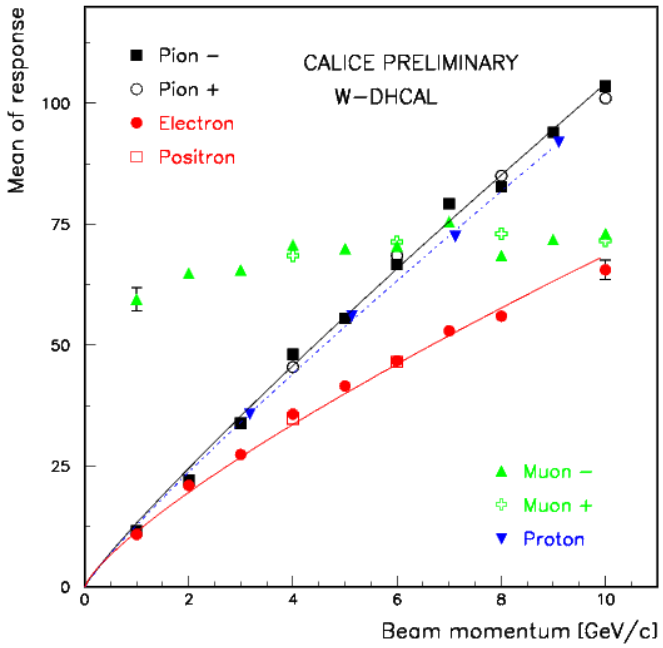

Figure 13. Mean of response to various particles in the beam as function of beam momentum at the PS. The lines are the results of fits with an empirical power law, $a \cdot p^b$, where p is the momentum.

Table III. Results of the fit of a power law $a \cdot p^b$ to the mean responses of electrons, pions and protons in the energy range of the PS, 1 – 10 GeV.

Particle	a	b
Electron	11.4	0.78
Pion	13.2	0.90
Proton	12.8	0.90

12. Measurements at the CERN SPS

The data at the SPS were collected in the H8 beam line and covered the energy range of 12 to 300 GeV. As an example, Fig. 15 shows the response to 30, 50, and 100 GeV negative pions. The data are compared to Monte Carlo simulations (rescaled by about - 16% to match the data). The selection for this plot includes a longitudinal containment cut requiring no hits in the last four layers of the TCMT. Nevertheless, the data show a tail towards lower hit numbers increasing with energy, which is also visible in the simulation, albeit not as pronounced. The reasons for the tail are not entirely understood. Reweighting the hits in the two parts of the TCMT to account for the different sampling ratios of the TCMT by minimizing the overall resolution, reduces the tail somewhat, but does not result in symmetric distributions. In the following the Gaussian fits to the number of hits are performed only over the symmetric part of the distributions.

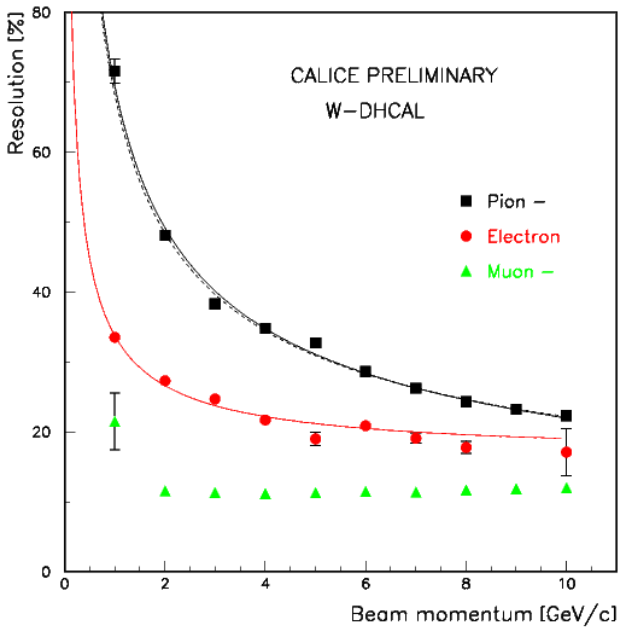

Figure 14. Resolution (relative width of the fitted Gaussian functions) versus beam momentum for negative particles as measured at the PS. The values have been corrected for the observed non-linearity of the response. The solid lines are the results of fits of the quadratic sum of a stochastic and linear term to the resolution for electrons (red) and negative pions (black). The black dashed curve is the result of a fit of the negative pion resolutions to the stochastic term only.

Table IV. Parameters of the fitted resolution functions for the PS data.

Particle	Constant term [%]	Stochastic term [%]
Electrons	16.6	29.4
Pions	0.0	69.5
	5.4	68.0

The mean response as function of beam momentum over the entire momentum/energy range of the PS and SPS is shown in Fig. 16. The effects of saturation noted with the PS data are also visible at higher energies. Empirical fits to a power law seem to describe the data adequately. The resulting parameters of the fits are summarized in Table V.

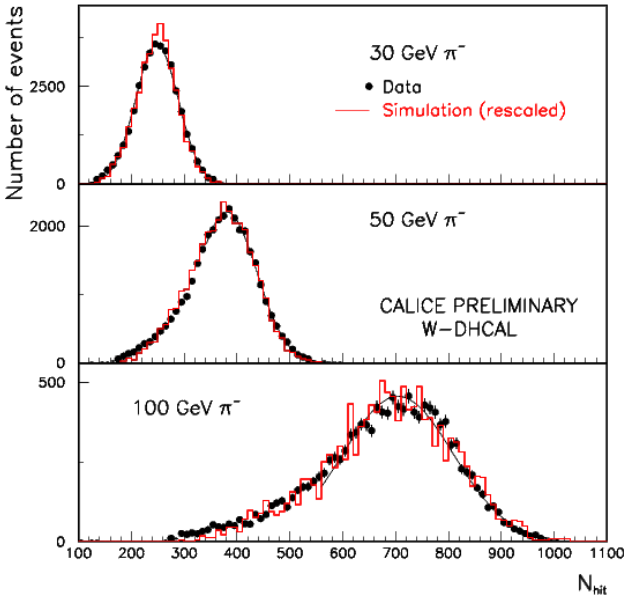

Figure 15. Distribution of number of hits for 30, 50, and 100 GeV negative pions, as measured (black dots) and simulated (red histogram). The simulation has been rescaled by about -16% to match the peak of the measured distribution. The black line is the result of a Gaussian fit to the data.

13. Conclusions

A preliminary analysis of the data collected at CERN in 2012 with the DHCAL inserted into tungsten absorber plates has been presented in this note. The present analysis was performed without calibration of the response of individual RPCs.

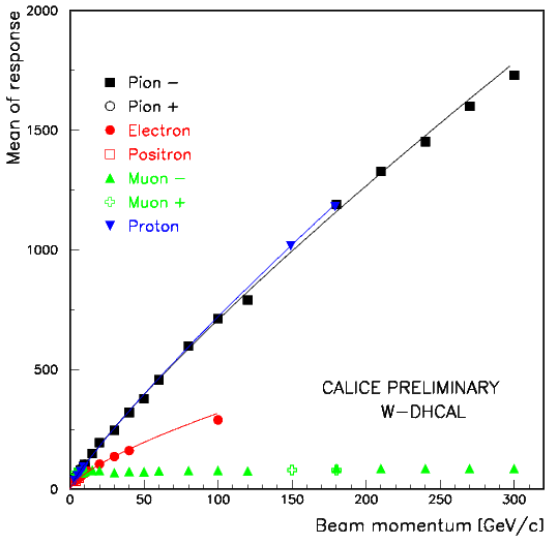

Figure 16. Mean response versus beam momentum for various particles as measured in the PS and SPS beams. The lines are the results of emprical fits by a power law, $a \cdot p^b$, where p is the particle momentum.

Table V. Parameters of the fits of the mean response to a power law $a \cdot p^b$ in the energy range of 1 – 300 GeV.

Particle	a	b
Electron	12.7	0.70
Pion	14.7	0.84
Proton	13.6	0.86

Compared with the results obtained with steel absorber plates [3], a number of observations can be made:

- At a given momentum the average number of hits is significantly smaller with tungsten than with steel absorber plates, of the order of 30% less.
- The response to pions (and electrons) deviates from a straight line already at low momenta (i.e. below 10 GeV/c). This is due to the higher density of showers in tungsten absorbers. These effects can be mitigated with smaller readout pad sizes, e.g. 0.5×0.5 cm^2, as was seen in simulations (not presented here).
- The resolutions are also somewhat inferior to what was obtained with steel plates. In the momentum range of the PS a stochastic term of ~68% added in quadrature to a constant term of 5 - 6% describes the measured resolutions for negative pions. For steel the corresponding values are ~56 % and 9 - 10 % respectively.
- Software compensation techniques, successfully applied to the CALICE AHCAL data [13], are expected to improve both the linearity and the resolutions.

References

1. J. Repond and CALICE, 'Analysis of DHCAL Muon Data', CAN-030.
2. L. Xia and CALICE, 'DHCAL Noise Analysis', CAN-031.
3. B. Bilki and CALICE, 'DHCAL Response to Positrons and Pions', CAN-032.
4. C. Adloff et al., 'Construction and Commissioning of the CALICE Analog Hadron Calorimeter Prototype', 2010 JINST 5 P05004.
5. A. Lucaci-Timoce and CALICE, 'Shower Development of Particles with Momenta from 1 to 10 GeV in the CALICE Scintillator-Tungsten HCAL', CAN-036.
6. J. Hoff et al., 'DCal : A Custom Integrated Circuit for Calorimetry at the Linear Collider', Proceedings of the 2005 IEEE Nuclear Science Symposium, Puerto Rico (2005).
7. B. Bilki et al., 'Measurement of the Rate Capability of Resistive Plate Chambers', JINST 4 P06003 (2009).
8. D. Dannheim, W. Klempt, and E. van der Kraaij. 'Beam tests with the CALICE tungsten analog hadronic calorimeter prototype.' CERN LCD-Note-2012-002.
9. S.Agostinelli et al., 'GEANT4 : A simulation toolkit', Nucl. Instrum. Meth. **A506** (2003), 250.
10. I. Ambats et al., 'Cosmic Ray Tests of the ZEUS Barrel Calorimeter Modules', Nucl. Instrum. Meth. **A320** (1992), 161.
11. GEANT4 simulation studies with 0.5×0.5 cm^2 pad readout together with tungsten absorber plates significantly improved the linearity and resolution for both electrons and pions.
12. See e.g., N.Akchurin et al., Nucl. Instr. Meth. **A537** (2005), 537.
13. C. Adloff et al., 'Hadronic Energy Resolution of a Highly Granular Scintillator-Steel Hadron Calorimeter using Software Compensation Techniques', 2012 JINST 7 P09017.